

Photocatalytic activity and colloidal stability of various combinations of TiO₂/SiO₂ nanocomposites

A. Khadem-Hosseini¹ · S. M. Mirabedini¹ · S. Pazokifard¹

Received: 25 September 2015 / Accepted: 28 November 2015 / Published online: 16 December 2015
© Springer Science+Business Media New York 2015

Abstract In this study, various combinations of TiO₂ and SiO₂ nanoparticles were prepared using different methods. TiO₂ and SiO₂ nanoparticles were separately modified by tetraethyl orthosilicate and titanium tetraisopropoxide, respectively. SiO₂/TiO₂ nanocomposite was synthesized through a two-step sol–gel route. A physical blend of TiO₂/SiO₂ nanocomposite was also prepared. The nanoparticles were characterized using FTIR spectroscopy, thermal gravimetric analysis, and X-ray diffraction technique. Specific surface area of the nanoparticles was determined using Brunauer, Emmett, and Teller method. The colloidal stability of various nanoparticles was investigated visually and instrumentally in an aqueous media. Photocatalytic activity of nanoparticles was studied through photo-degradation of rhodamine-B dyestuff, in aqueous solutions under UVA irradiation. The results showed improvement of dispersion stability along with the decrease in photocatalytic activity for silica-grafted TiO₂-nanoparticles in aqueous solutions compared with the untreated particles. However, titania-grafted SiO₂ nanoparticles showed reduced colloidal stability and better photocatalytic activity than their untreated counterparts. The synthesized SiO₂/TiO₂ nanocomposites revealed the enhanced both photocatalytic activity and colloidal stability among the others.

Introduction

Nowadays, air pollution particularly in urban areas poses serious risk to human health and environment. Many efforts have been carried out to reduce the harmful effect of this phenomenon [1–4]. For this purpose, photocatalytic titania nanoparticles have been used extensively in different applications to reduce air pollution in urban landscapes and keep clean the buildings' appearance [5]. TiO₂, in anatase crystalline form, is recognized as a golden standard among the semiconductor materials [6, 7], owing to its unique properties, appropriate cost/performance balance, chemical stability and biocompatibility [8]. Photocatalytic TiO₂ nanoparticles have many potential applications as catalysts or catalyst supports in different fields such as water purification [9], waste-water treatments [10], and self-cleaning coatings [11].

Despite the high photocatalytic activity, and due to the extremely high ratio of surface-area/particle-size, TiO₂ nanoparticles illustrate poor dispersion stability in the aqueous solutions and the particles tend to strongly agglomerate, upon agitation process stops [12]. Moreover, addition of photoactive TiO₂ nanoparticles into or deposited on the surface of polymeric coatings has many shortcomings, due to possible degradation or breaking C–C bonds of the host polymer matrix [13, 14].

Several efforts have been carried out to enhance dispersion stability of TiO₂ nanoparticles in the aqueous media [13] and to adjust their photocatalytic activity [12]. In particular, silica-based treatments of the nanoparticles have been received intensive attentions because of their advantages such as simplicity, low cost and possibility of processing at ambient temperature [12, 13]. Several reports are available concerning preparation and photoactivity of TiO₂/SiO₂ compounds [15–23]. The influence of synthesis

✉ S. M. Mirabedini
sm.mirabedini@ippi.ac.ir

✉ S. Pazokifard
s.pazokifard@ippi.ac.ir

¹ Color, Resin & Surface Coatings Department, Iran Polymer and Petrochemical Institute, P.O. Box 14965-115, Tehran, Iran

method on the physicochemical properties of titania–silica compounds, and consequently its effect on the photocatalytic activity of the particles has been pointed out by Aguado et al. [24]. They also reported that photocatalysis of the semiconductor is the most relevant mechanism for the explanation of photoactivity of $\text{TiO}_2/\text{SiO}_2$ materials. In another work, Rasalingam et al. [25] showed that the content of Ti–O–Si species and appropriate distribution of titania on the silica support, are the most effective parameters on the photoactivity of these compounds. It has been also emphasized [21, 26] that silica-embed particles enhanced the crystalline phase changing transition temperature. In spite of numerous reports concerning of preparation and application of titania/silica compounds, there are only a few published works on simultaneous study of colloidal stability and photoactivity of various combinations for $\text{TiO}_2/\text{SiO}_2$ in aqueous media. Improving dispersion stability of photocatalytic nanoparticles leads to increased available surface area for more photon absorption by pollutant molecules, and as result of this, photodegradation of pollutants leads to small amounts of relatively benign compounds.

In this study, various combinations of titania–silica nanoparticles were prepared using different methods, and then photocatalytic activity and dispersion stability of resultant nanoparticles were investigated in aqueous solutions. Here, in addition the synthesis of $\text{SiO}_2/\text{TiO}_2$ nanocomposites has also been reported with a high surface area, appropriate dispersion stability, and improved photocatalytic properties using a superficial method that combines sol–gel route and calcination procedure.

Experimental

Materials

TiO_2 nanoparticles, Aeroxide P25, with an average particle size of 30 nm, a specific surface area of $50 \pm 15 \text{ m}^2 \text{ g}^{-1}$ and an anatase/rutile ratio of 70/30 [25] to 80/20 [26], and fumed silica nanoparticles (Aerosil 200, with an average particle size of 12 nm and specific surface area of $200 \pm 25 \text{ m}^2 \text{ g}^{-1}$) were supplied by Evonik Industries (Degussa GmbH). Tetraethylorthosilicate (TEOS, 98 wt%) and titanium tetraisopropoxide (TTIP, 98 wt%) were purchased from Fluka and used as precursors for surface treatment of SiO_2 and TiO_2 nanoparticles, respectively. Rhodamine B dyestuff (RhB), as a pollutant model, was obtained from Ciba-Gigy. Nitric acid (65 wt%), acetyl acetone (AA), ammonium hydroxide (28 wt%), ethanol, and isopropanol were provided by Merck Chemicals. Other chemicals were of reagent grades and used without further purification.

Nanoparticles surface treatments

A Surface treatment of TiO_2 nanoparticles was performed using a two-stage sol–gel route [27]. TiO_2 nanoparticles (1.5 g) were dispersed in 33 mL ethanol via sonication process for 15 min (Bandelin, SONO PULS-UW 2200, using KE-76 probe) at 70 W, and 0.7 s pulse on and 0.3 s pulse off. 3 mL TEOS was added to the dispersion during the sonication process, 1 mL per 5 min interval. The molar ratio of P25:TEOS was adjusted as 12:1 [27]. pH was adjusted to about 9–10 by adding 0.9 mL ammonium hydroxide to the dispersion. The dispersion was then magnetically stirred in a dark environment at ambient temperature for 18 h, centrifuged (Rotina 3800 Hetich) at 7000 rpm for 10 min, and rinsed with ethanol four times. The sediments were dried in an oven at 50 °C for 48 h.

B The surface treatment of silica nanoparticles was performed using a two-step sol–gel process [28]. In the first step, TTIP was pre-hydrolyzed. For this purpose, 1.96 mL TTIP and 1.1 mL AA (0.6 TTIP: 1.0 AA mole ratio) were added to 10 mL ethanol. The solution was stirred at ambient temperature ($23 \pm 2 \text{ }^\circ\text{C}$) for 2 h. In the second step, 1 g Aerosile 200 was dispersed in the mixture of 18 mL ethanol and 2 mL distilled water under sonication process for 15 min. pH of the dispersion was adjusted to around 6 using a few droplets of ammonium hydroxide solution. Afterward, the pre-hydrolyzed solution was added dropwise to the dispersion within 1 h. The molar ratio of SiO_2 :TTIP: H_2O was adjusted as 1:4:16 [29]. For completion of the treatment, the resultant dispersion was refluxed at 85 °C for 6 h. Finally, it was centrifuged (7000 rpm) for 10 min, and the residue was rinsed with ethanol four times. The precipitates were dried at 50 °C for 24 h.

C $\text{TiO}_2/\text{SiO}_2$ nanocomposite sample was synthesized as per the following procedure: TTIP and TEOS were pre-hydrolyzed in two distinct pots. Accordingly, 1.8 mL TTIP was dissolved in a mixture of 0.46 mL ethanol and 3.11 mL isopropanol by gentle magnetic stirring at ambient temperature ($23 \pm 2 \text{ }^\circ\text{C}$) for 1 h (solution A). In parallel, hydrolysis of TEOS (0.9 mL) was performed in an acidic condition (pH 2), containing 27 mL distilled water and a few droplets of HNO_3 (solution B). Pre-hydrolyzed TTIP solution was then added dropwise into the solution B. The molar ratio of TTIP:TEOS was considered as 60:40. The solution was then refluxed at 85 °C for 6 h. The sediment was rinsed thoroughly with ethanol several times, filtered, and dried at 50 °C for 24 h. for BET specific surface area measurement and XRD analysis, the prepared $\text{TiO}_2/\text{SiO}_2$ nanocomposites were calcinated at 600 °C for 3 h [30].

D Physical blending of TiO_2 and SiO_2 nanoparticles with weight ratio of 1:1 was prepared by mixing and grinding of the nanoparticles in a pestle for 30 min. Sample coding for all used and prepared nanoparticles is listed in Table 1.

Table 1 Samples' coding of various nanoparticles

No.	Sample coding	Description of sample preparation
1	UT	Untreated titania nanoparticles
2	US	Untreated silica nanoparticles
3	MT	TEOS-treated TiO ₂ nanoparticles
4	MS	TTIP-treated SiO ₂ nanoparticles
5	TSb	Physical blending of TiO ₂ –SiO ₂ nanoparticles
6	TSc	Nanocomposites of TiO ₂ –SiO ₂ nanoparticles
7	Calc. MS	Calcination of MS nanoparticles at 600 °C for 3 h
8	Calc. TSb	Calcination of TSb nanoparticles at 600 °C for 3 h

Characterization of nanoparticles surface treatment

Possible chemical interactions between precursors and nanoparticles were evaluated using FTIR spectroscopy using a Bruker IFS 484 FTIR spectrometer, collecting 16 scans in the 600–4000 cm⁻¹ range with 4 cm⁻¹ resolution, using KBr disk technique.

The thermal behavior of various nanoparticles was studied using a TGA-PL-1500 analyzer under N₂ atmosphere from room temperature to 600 °C with a heating rate of 10 °C min⁻¹. Before testing, the samples were dried in a low pressure oven at 80 °C for 2 h.

The intensities of crystalline phases of various nanoparticles were determined by X-ray diffraction (XRD) method. XRD pattern of nanoparticles was recorded on a Shimadzu XRD-6000 using Fe K α ($\lambda = 1.93604 \text{ \AA}$) irradiation, with flow intensity and voltage of 50 mA and 30 kV, respectively, in the degree range of 20°–70°.

Specific surface area of the samples was determined via N₂ adsorption according to Brunauer, Emmett, and Teller (BET) analysis method. Samples were conditioned at 120 °C for 2 h before testing, and then adsorption/desorption isotherms were determined using a Quantachrome CHEMBET 3000 at 196 °C.

Dispersion stability of nanoparticles

Dispersion stabilities of various nanoparticles were evaluated in distilled water. Nanoparticles with a concentration of 1 g L⁻¹ were dispersed in distilled water via sonication process for 15 min. The dispersion was then allowed to stand for 20 days, after which sedimentation behavior was visually evaluated.

Dispersion stability of the nanoparticles in distilled water (1 g L⁻¹) was also studied using a LUMiReader[®] 416.1, LUM separation analyzer, working in the light intensity of 25 % and tilt angle of 0°. The total test duration was 3.5 h for TEOS-treated nanoparticles and 72 h for other samples including 256 intervals.

Photocatalytic activity of nanoparticles in aqueous solutions

Optical absorbances of various nanoparticles with concentration of 20 mg L⁻¹ in distilled water were evaluated using a Shimadzu UV–Vis spectrophotometer (UV-1650-PC model) between 200 and 700 nm. The photocatalytic activity of nanoparticles was also evaluated in an aqueous solution in the presence of RhB dyestuff, as a photo-degradable model. Each sample (20 mg L⁻¹) was separately dispersed in distilled water containing 12.5 mg L⁻¹ RhB via sonication process for 15 min. The dispersion was exposed to UVA irradiation (340 nm, 0.89 W m⁻²) in a QUV chamber (QUV/Spray accelerated weathering device from Q-Panel Co.) at 45 °C until completion of RhB photo-degradation. At different time intervals, the nanoparticles were separated from the dispersion via centrifugation at 8000 rpm for 15 min. The photocatalytic decomposition of RhB in the resultant solutions was recorded on UV–Vis spectroscope at wavelengths in the range of 400–700 nm. Reduction in a characteristic absorption peak of RhB at wavelength of 554 nm was considered as the photo-degradation index. RhB photo-degradation % was determined using Eq. 1:

$$\text{RhB photo-degradation (\%)} = \frac{A_{\text{ex}}}{A_i} \times 100, \quad (1)$$

where A_i and A_{ex} represent maximum absorbance % at the wavelength of 554 nm at initial and different UVA exposure times, respectively.

Results and discussion

FTIR spectroscopy

Figure 1 shows the FTIR spectra of TTIP, TEOS, and various nanoparticles. In FTIR spectrum of pristine TiO₂ nanoparticles (Fig. 1a), broad absorption peaks in the

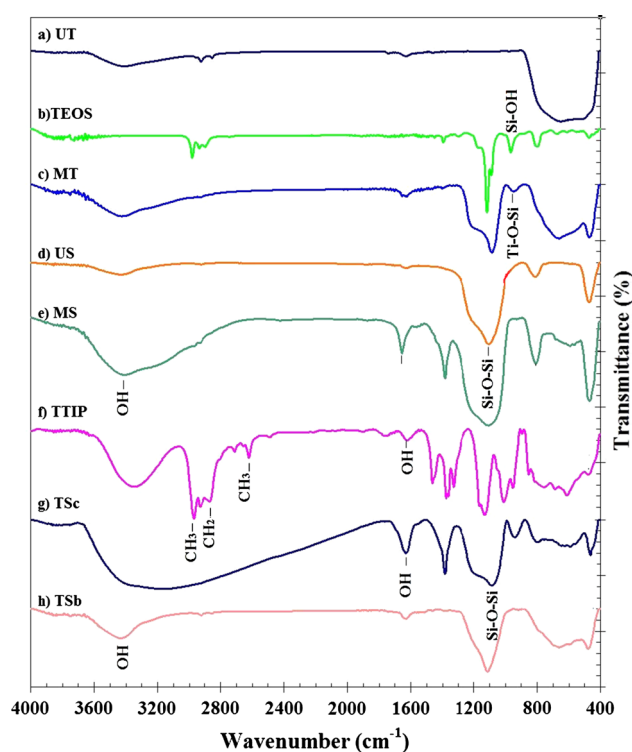


Fig. 1 FTIR spectra of various nanoparticles and precursors

region of $400\text{--}800\text{ cm}^{-1}$ are attributed to Ti–O and Ti–O–Ti bonds [18, 31], indicating crystalline TiO_2 [15]. The absorption peaks around $935\text{--}950\text{ cm}^{-1}$ (Fig. 1b) are ascribed to symmetric vibration of Si–OH [15] bonds. The absorption bands around 3400 and 1600 cm^{-1} , observed in all spectra, are attributed to the stretching mode of the O–H bond related to the physically adsorbed water and bending vibration of the O–H bond of chemisorbed water, respectively [31, 32]. The broad and intensive O–H bond at around 3400 cm^{-1} in FTIR spectra of MS and TSc samples (Fig. 1e, g) is due to higher concentration of hydroxyl groups on the surface of the samples. In FTIR spectrum of TTIP sample (Fig. 1f), the absorption peaks at around 2624 , 2864 , and 2966 cm^{-1} are attributed to symmetric and asymmetric stretchings of CH_2 and CH_3 bonds [33, 34]. In FTIR spectra of MT and TSc samples (Fig. 1c, g), the characteristic peaks in the range of $950\text{--}960\text{ cm}^{-1}$ belong to the vibration of Si–O–Ti bond [18, 33, 35]. This good-quality bond plays an important role in the photocatalytic activity of $\text{TiO}_2/\text{SiO}_2$ compounds [25]. This peak is more intensive for $\text{SiO}_2/\text{TiO}_2$ composite sample (Fig. 1g) compared with its counterpart in FTIR spectrum of MT sample (Fig. 1c). As shown in Fig. 1c, e, g, and h, for all silicate structures, the absorption peaks appeared at regions of $1000\text{--}1130$ and $450\text{--}550\text{ cm}^{-1}$, which corresponded to the asymmetric vibration of Si–O–Si [15, 17] stretching and the symmetric stretching vibration of Si–O–

Si, respectively [36]. These results confirm chemical bonding of SiO_2 on the TiO_2 particles for MT and TSc samples [15, 33].

Thermal gravimetric analysis

TGA thermographs of different nanoparticles are depicted in Fig. 2, and the test results are tabulated in Table 2. For all samples, the weight loss occurred in three steps. Weight loss observed at low temperature ($25\text{--}200\text{ }^\circ\text{C}$) can be attributed to the elimination of physically adsorbed water from the samples [27, 37]. These were about 0.65 and 1.69 wt% for untreated SiO_2 and TiO_2 nanoparticles and 3.44 and 3.69 wt% for MS and TSc samples, respectively. These results indicate higher hydrophilic characteristic of MS and TSc samples, which are in agree with the FTIR analysis outcomes. The second step in weight loss occurred in the temperature range of $200\text{--}450\text{ }^\circ\text{C}$. For different samples, the weight losses in this temperature zone were varying between 0.91 and 6.98 wt%. For untreated SiO_2 and TiO_2 nanoparticles, these were about 0.91 and 2.28 wt%, respectively, which might be due to the formation of water molecules from the condensation of hydroxyl groups on the nanoparticles' surface [27]. Here, the weight losses for MS (6.98 wt%) and TSc (6.41 wt%) samples (Fig. 2e, f) can be attributed to the combustion of unhydrolyzed isopropoxide compounds [38] and to a lesser extent, to the removal of solvents and other residual organic compounds from the nanoparticles' surfaces [39]. Jung et al. [40] showed relatively slight weight loss after $340\text{ }^\circ\text{C}$ for US or UT samples, ascribed to the water molecules formed from condensation of hydroxyl groups on the particle's surface (SiOH or TiOH). For all samples, the condensation of germinal and vicinal OH groups on the surface of SiO_2 and

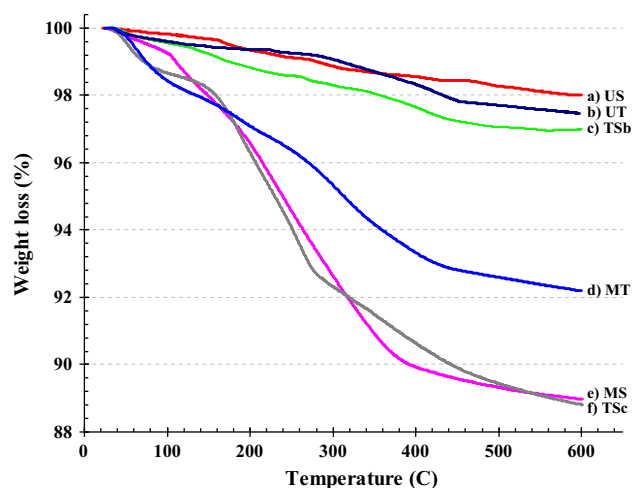


Fig. 2 TGA thermographs of various nanoparticles' samples

Table 2 Weight loss wt% for various nanoparticles obtained from TGA and BET specific surface area values for different nanoparticles

Sample coding	TGA results			Total weight loss (%)	BET specific surface area values BET surface area (m ² g ⁻¹) (average of three measurements)
	Temperature ranges (°C)				
	25–200	200–450	450–600		
UT	1.69	2.28	0.03	4.00	53.6 ± 2.1
US	0.65	0.91	0.42	1.98	174.6 ± 8.6
TSb	1.17	1.59	0.22	2.99	114.1 ± 5.4
MT	2.92	4.27	0.63	7.82	134.3 ± 8.9
MS	3.44	6.98	0.60	11.02	–
TSc	3.69	6.41	1.09	11.19	–
Calc. MS	–	–	–	–	229.5 ± 7.5
Calc. TSc	–	–	–	–	331.4 ± 11.3

TiO₂ nanoparticles can also be reason for the weight loss at this temperature zone [37].

The weight loss observed in the last temperature region (ca. 450–600 °C), is believed to be due to the oxidation and de-hydroxylation of the organic molecules [27, 31] and/or de-bonding and degradation of the grafted layer on the nanoparticles' surface [27]. While, as is also reported [32], the weight loss above 500 °C is related to the condensation of hydroxyl groups linked to SiO₂ or TiO₂ substances. The maximum weight loss belongs to TSc sample (1.09 wt% in third zone and 11.19 wt% in total), indicating chemical interactions between TEOS and TTIP functional groups [41]. Relatively high weight losses for TSc and MS samples, ca 11.19 and 11.02 wt%, respectively, suggest more organic compounds on the surface and also higher hydrophilic characteristic behavior of these nanoparticles compared with the others.

X-ray diffraction

XRD patterns of various nanoparticles are shown in Fig. 3. For MS and TSc samples, XRD tests were performed before and after calcination at 600 °C for 3 h. In XRD pattern of SiO₂ nanoparticles (Fig. 3a), no characteristic crystalline peak can be observed due to amorphous behavior of the sample. The result also reveals that by TTIP treatment (Fig. 3b), no significant crystalline phase appeared in the XRD-pattern of silica nanoparticles. The reaction of TTIP with silica nanoparticles may prevent the formation of titania nanoparticles. However, the calcination process improved the crystallinity of the nanoparticles (Fig. 3c), and the amorphous TiO₂ changed into the anatase crystalline phase [42]. The XRD pattern of the TSc sample prior to calcination (Fig. 3d) shows an amorphous phase, while that calcinated at 600 °C (Fig. 3e) is identified as a crystalline anatase phase. The anatase structure is the main phase of the TiO₂/SiO₂ nanoparticles, and no significant

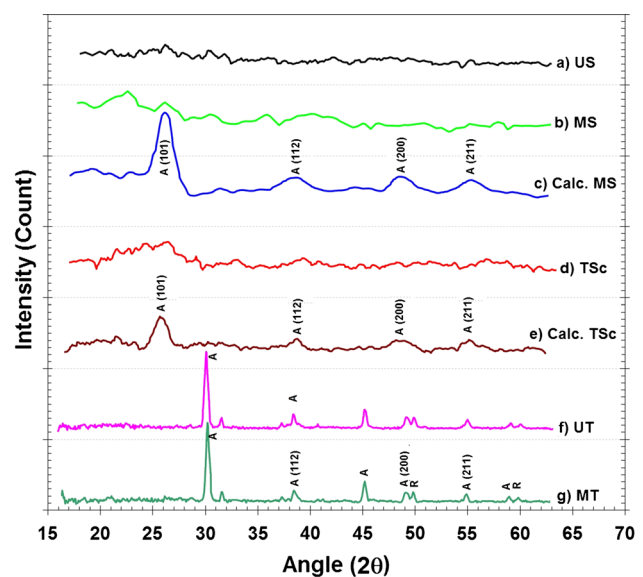


Fig. 3 XRD patterns of (a) US, (b) MS, (c) calcinated MS, (d) TSc, (e) calcinated TSc, (f) UT, and (g) MT

rutile phase appeared in the XRD pattern. The results showed that the maximum intensity of major anatase phases corresponded to UT sample (Fig. 3f). It is reported [43] that P25 is quite a crystalline substance with an anatase/rutile ratio of 81/19. The peaks attributed to neat anatase phase of TiO₂ appeared at around 2θ of 25°, 38°, 48°, and 55° that are attributed to (1 0 1), (1 1 2), (2 0 0), and (2 1 1) planes, respectively. The peaks related to neat rutile phase appeared at around 2θ of 27°, 35°, 41°, and 57°, which are assigned to (1 1 0), (1 0 1), (1 1 1), and (2 2 0) crystalline planes, respectively. The particles' crystallinity was quantitatively estimated with the relative intensity of the (1 0 1) diffraction peak of the pure anatase [44]. By TEOS treatment, Fig. 3f and g, no considerable new peak merged in the XRD pattern of TiO₂ nanoparticles; however, the intensity of peaks attributed to anatase

plane (1 0 1) was slightly decreased. Based on XRD analysis results, it can be concluded that the interactions of TEOS with TiO₂ nanoparticles occurred mostly at the nanoparticles' surface. There is probably no alteration in the internal crystalline structure of the nanoparticles and also no dissolution or growth of the titania before or after TEOS treatment. It is summarized that for MS and TSc samples, the majority of crystalline structure phase is anatase; thus, higher photocatalytic activity is predicted for these samples from XRD outcomes.

Specific surface area measurement

Specific surface area measurement results (determined by means of BET method) for different samples are listed in Table 2. Specific surface area is a characteristic structural parameter of particles, which can be used to differentiate the condition of a grafted layer on its surface [13]. Increasing specific surface area of the treated nanoparticles may be an indication of surface grafting of the nanoparticles. As is evident, the BET values of neat TiO₂ and SiO₂ nanoparticles were increased from 53.6 to 134.3 m² g⁻¹ and from 174.6 to 229.5 m² g⁻¹, respectively, probably due to silica and titania grafting on the nanoparticles' surface. The grafting makes the nanoparticles' surface irregular and rough; hence, increase in the specific surface area is anticipated. The highest specific surface area was obtained for TiO₂/SiO₂ nanocomposites. These results can be attributed to the finer particles containing silica and titania dopants [23, 39]. It should be pointed out that the higher surface area leads to the higher photocatalytic reactions due to the increasing contact area of the catalyst with the substrates, where RhB molecules must be initially adsorbed by the photocatalyst nanoparticles. Therefore, higher photocatalytic activities for MS and TSc samples are expected from the BET results.

Dispersion stability study

The results for dispersion stability analysis of the nanoparticles are shown in Fig. 4. Various nanoparticles showed different degrees of stability in the aqueous solutions. Sedimentation of UT sample occurred rapidly and completed within 24 h. TiO₂ nanoparticles have poor dispersion stability and shows tendency to flocculation very quickly [27, 45]. However, dispersion of TEOS treated titania nanoparticles (MT) was more stable due to the silica grafting on the particles' surface and formation of static electricity repulsion between the particles [27]. For this sample, sedimentation process was completed after 20 days. Suspension containing neat silica nanoparticles was stable during the test period, and no sediment was observed even at the end of test completion after 20 days.

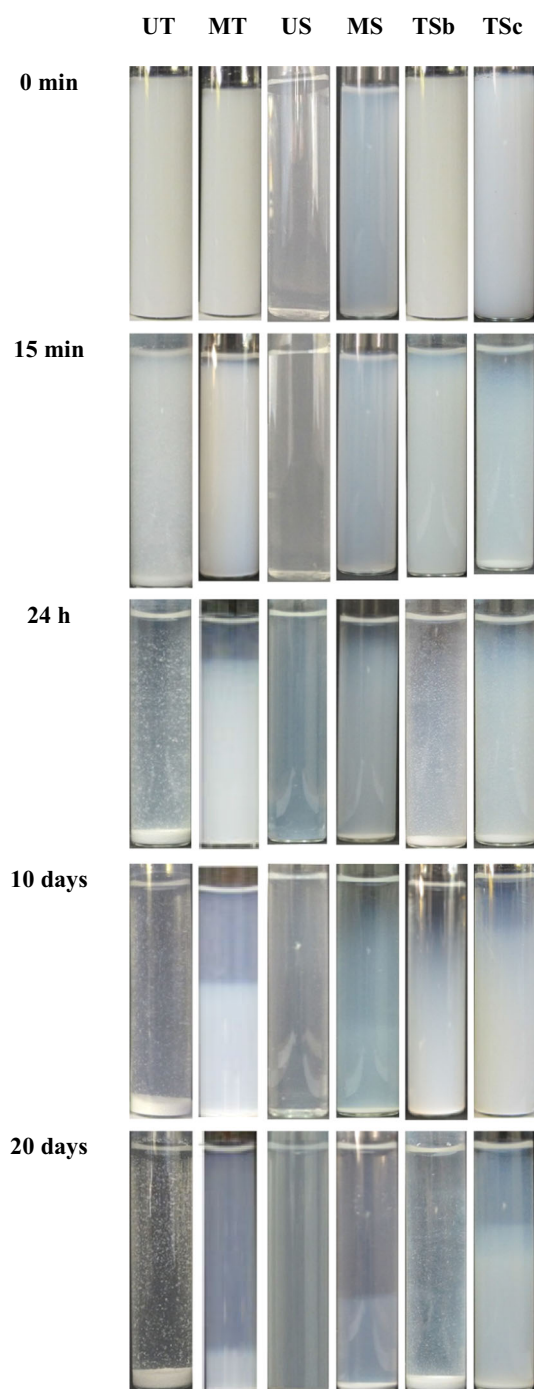


Fig. 4 Visual observations of sedimentation of 1 wt% different nanoparticles in distilled water during 20 days

The dispersion of neat silica nanoparticles showed proper stability in aqueous media because of existence of hydroxyl group on the particles' surface [46]. For dispersion containing MS sample, sedimentation was launched after 24 h, and it was completed within 20 days (the upper part of the dispersion was still somewhat turbid). TSc-containing dispersion was more stable than its counterpart having TSb

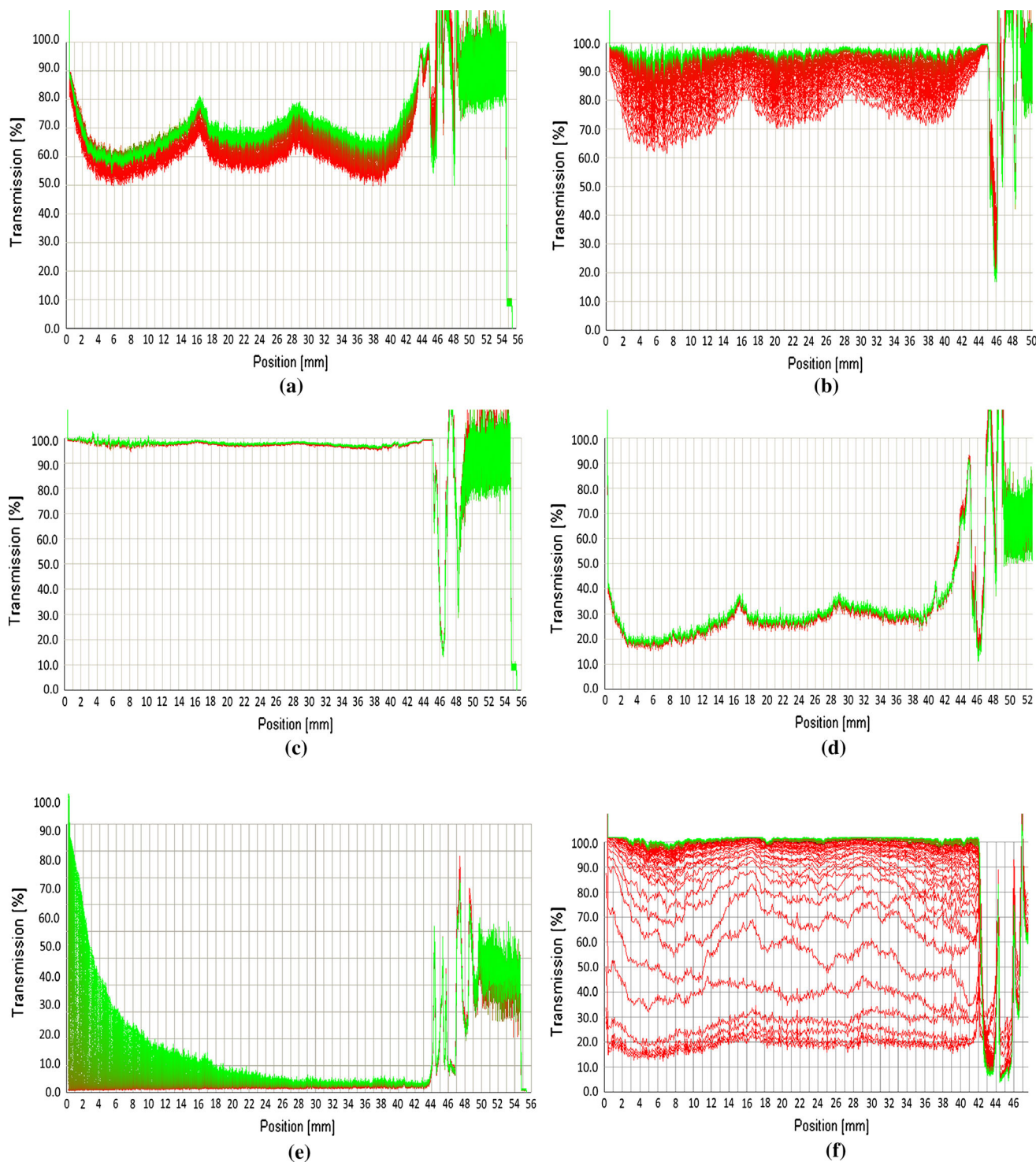


Fig. 5 Separation analysis in LUMiReader[®]. Sedimentation behavior of aqueous dispersion containing 1 g L⁻¹ of **a** MS, **b** TSc, **c** US, **d** TSb, **e** UT, and **f** MT; test duration: 72 h for MT and 3.5 h for other samples

nanoparticles. Grafted silica on the nanoparticles surface probably operates as an anchoring group making particle-to-particle contact difficult. It is believed that sedimentation phenomenon for TSb dispersion is mostly through

coagulation process, while for TSc dispersion, it is via flocculation process; therefore, it makes TSc dispersion more stable. These results reveal that the presence of SiO₂ on the surface of titania nanoparticles hindrance

agglomeration of the nanoparticles. The trend for increasing dispersion stability is ordered as follows: $US > MT > MS > TSc > TSb > UT$.

Figure 5 shows the separation analysis results obtained from a LumiReader[®] analyzer, which illustrates the sedimentation behavior of various nanoparticles in the distilled water at different heights of test tube (positions). Each diagram in the Fig. 5 shows one examine by the apparatus in defined time intervals. As shown in the figure, the sedimentation rate for UT sample is very fast so that the light transmission becomes almost 100 % within 3.5 h (Fig. 5a), whereas this has not happened for TSc sample even after 72 h (Fig. 5b), which indicates the enhancement in the dispersion stability of TSc sample. The LumiReader[®] analyzer used as an instrument for the measurement confirmed the visual observation results.

Photo-degradation of RhB dyestuff

The UV–Vis spectra of different nanoparticles are shown in Fig. 6. UT and US nanoparticles showed the highest and the lowest values of UV absorption in UV region among the samples, respectively. The absorption values for modified and synthesized nanoparticles were significantly decreased in UV region in comparison with their untreated titania counterpart. Meanwhile, calcinated MS sample has been shown as an acceptable absorption in the UV region, due to changes in surface characteristics of nanoparticles. Decreasing absorption in UV region may cause reduction in photocatalytic activity; therefore, for MT and TSc nanoparticles with decreased UV absorption, reduced photocatalytic activity is expected compared with TSb and

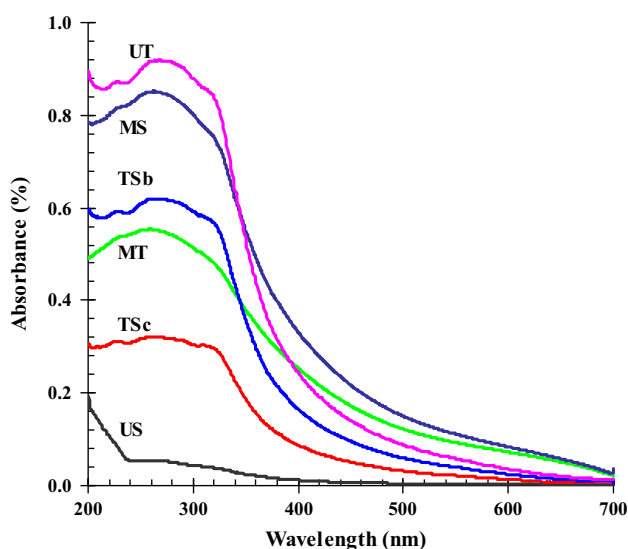


Fig. 6 UV–Vis spectra of aqueous solution (0.02 g L^{-1}) of different nanoparticles

TSc nanoparticles. It should be noted that decrease in aggregates' size due to the surface modification also leads to lower light scattering and less absorption [27, 47].

In respect of the applicative aspect, RhB dyestuff has been used as a pollutant model, and the photo-degradation of this model was studied in the presence of different nanoparticles under UV irradiation in an aqueous media. The photo-degradation process was evaluated in two approaches: taking photographs of the specimens at different time intervals and the measuring of UV–Vis tendency of RhB concentration in the aqueous solution by means of UV–Vis spectrometry. The UV–Vis spectra of the RhB dyestuff in the aqueous solutions (12.5 mg L^{-1}) after nanoparticles' filtration, during various UVA exposure times, are illustrated in Fig. 7. Typical color changes during RhB photo-degradation process are also shown in Fig. 7(inset). Regarding the RhB dyestuff degradation, UT-containing dispersion showed the best photochemical activity (Fig. 7a). In the presence of UT nanoparticles, the photo-degradation and/or photobleaching of RhB were completed after 120 min under UVA irradiation, and an initially pink-colored liquid turned to a completely colorless solution. As expected, the discoloration efficiency of UT-containing sample was the highest among the other nanoparticles' dispersions. On the contrary, a significant reduction in photocatalytic activity was observed for MT sample (Fig. 7b), where the liquid dispersion containing MT showed discoloration after about 300 min. In fact, for initiation of photo-degradation process, RhB must be firstly adsorbed on the surface of TiO_2 nanoparticles, where it is then photo-degraded due to UVA excitation of TiO_2 . However, silica grafting on the surface of nanoparticles decreases the effective surface area of TiO_2 available for photon absorption by RhB [27] and as a consequence, the rate of RhB photo-degradation is reduced. The reduced photocatalytic activity of MT sample is perhaps owing to the decrease in active sites on the titania surface. No blue shift was seen in the spectra after UV irradiation expect small one for TSc sample. In this case, rhodamine as a remarkable intermediate compound can be generated [30]. On the other side, no photocatalytic activity was observed for US-containing suspension (Fig. 7c). In contrast, MS-containing sample showed a relatively comparable behavior, the colored suspension turned to white color after about 150 min (Fig. 7d). Significant comparable RhB photo-degradation was observed using UT and MS nanoparticles. For dispersion containing TSc sample, the initially pink solid turned to white color in about 240 min; however, the majority of color fading was occurred in first 120 min. Only dispersion containing US nanoparticles showed a minimum capability of degrading RhB, turning to a pale pink color after about 300 min of UVA irradiation. As has been reported in our previous study [33], neat RhB aqueous

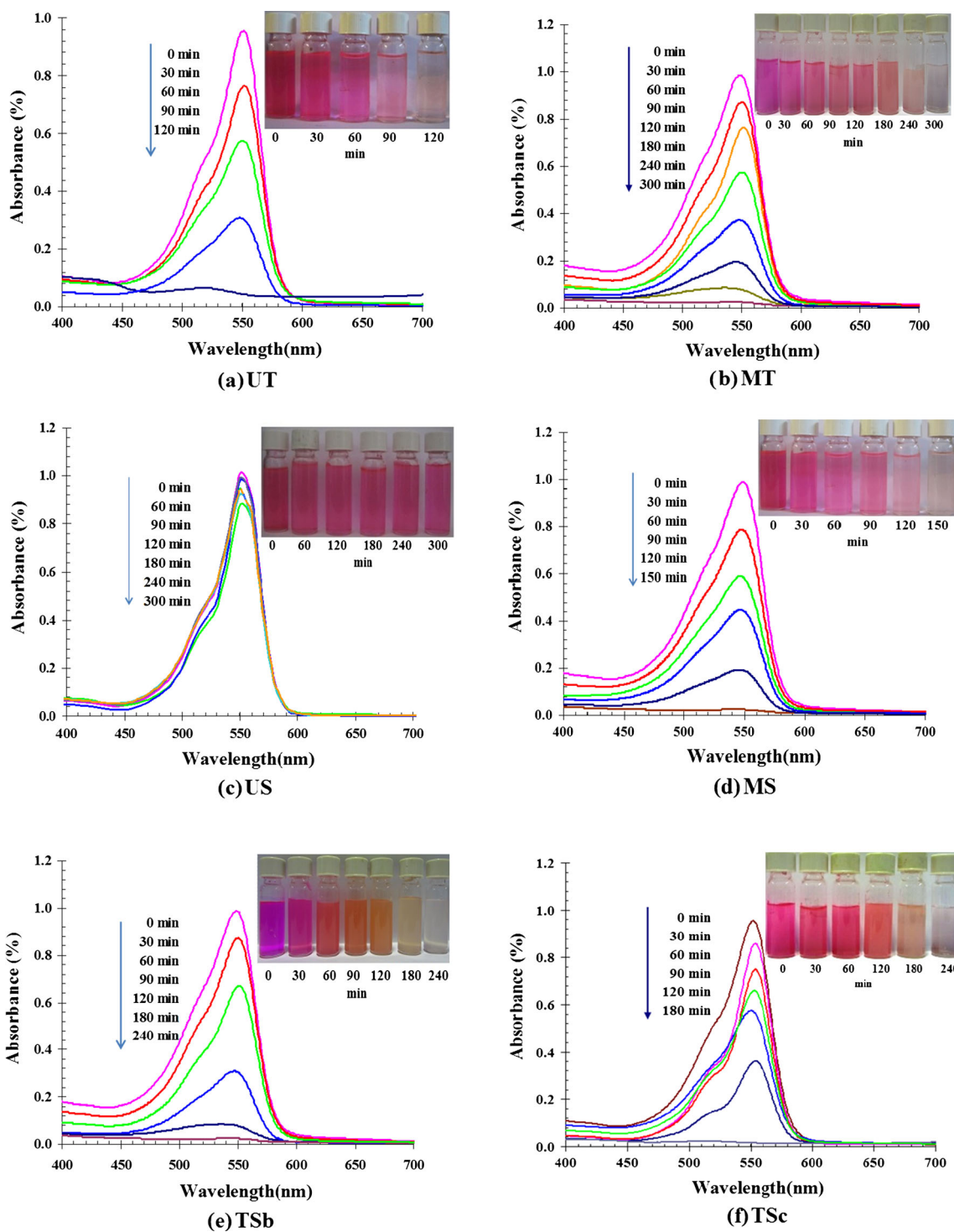


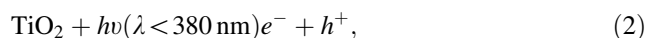
Fig. 7 The UV–Vis spectra and visual observation of RhB dyestuff in aqueous solutions (0.01 g L^{-1}) in the presence of **a** UT, **b** US, **c** TSb, **d** MS, **e** TSc, and **f** MT nanoparticles, during various UVA

exposure times. (Inset) Distinctive color changes during the photo-degradation process

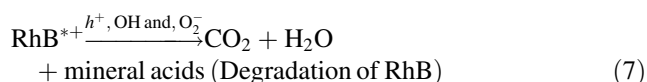
solution, in the absence of the photocatalyst nanoparticles, was not significantly affected by the UVA irradiation even after several hours. For the neat RhB solution, slight reduction in the intensity of absorption peak of RhB (not

shown here), can be due to photo-degradation of dyestuff itself, instead of photobleaching phenomenon. Photo-degradation of RhB under UVA exposure can be occurred via two different mechanisms, the formation of

electron/hole (e^- , h^+) pairs of semiconductor, owing to excitation of electron from valance bond to the conduction bond, and electron injection from the dyestuff orbital to the semiconductor conduction band [27]. The h^+ (valence band) can be able to produce hydroxyl radicals ($\cdot\text{OH}$) on the surface of TiO_2 nanoparticles and the conduction band (e^-) potentially is negative to reduce oxygen molecules to $\cdot\text{O}_2^-$. The photo-degradation mechanism of RhB can be shown in the following equations [28, 29, 48]:



The dyestuff matters (RhB) present at or near the surface of TiO_2 nanoparticles may be then attacked by $\cdot\text{OH}$ (hydroxyl radical) and are changed into harmless species (e.g., CO_2 , H_2O , etc.), as illustrated through the following equations [48, 49]:



The intensity of characteristic absorption peak at 554 nm regularly decreased during UVA irradiation as a result of decrease in the RhB concentration in the dispersion. These results can be used for comparison of photocatalytic activities of different nanoparticles in aqueous solutions. Figure 8 illustrates the determined photo-

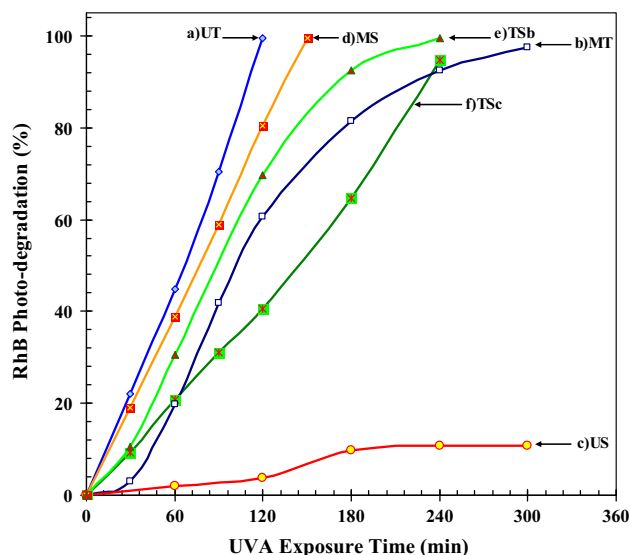


Fig. 8 Photo-derogation % of RhB during different UVA exposure times in the presence of various nanoparticles

degradation % of RhB dyestuff using Eq. 1 in aqueous solutions in the presence of various nanoparticles during 300-min UVA exposure time. The time required for completion of RhB degradation can be used for estimation of photocatalytic activity of nanoparticles. Higher surface area and more active sites caused more RhB absorption on the nanoparticles' surface, and consequently, higher intensity of active electron/hole leads to decrease in photo-degradation time. The photo-degradation of RhB solution in the presence of TSb sample is due to the existence of titania as a part of physical blending of nanoparticles. Based on the UV–Visible spectroscopy results, the order of RhB photo-degradation can be listed as UT (120 min), calcinated-MS (150 min), TSb (180 min), TSc (240 min), and MT (300 min). These results have good correspondence with XRD and BET results.

Conclusions

In this study, various combinations of $\text{TiO}_2/\text{SiO}_2$ nanoparticles were prepared using several methods with different degrees of titania content and anatase crystalline phase. FTIR and TGA analyses confirmed the surface modification of the TiO_2 nanoparticles and the effectiveness of the sol–gel route for the preparation of $\text{TiO}_2/\text{SiO}_2$ nanocomposites. Photocatalytic activity and colloidal stability of the nanoparticles in an aqueous media were investigated. Dispersion stability tests showed that silica-grafted nanoparticles had better stability in aqueous solution due to enhanced repulsion forces between particle and particle together. The results also revealed that the modified titania, in spite of good photoactivity, had poor dispersion stability, due to large surface area/particle size. Nanoparticles with enhanced specific surface area and increased anatase crystalline phase exhibited better photocatalytic activity. Among the other samples, the $\text{TiO}_2/\text{SiO}_2$ nanocomposites depicted reasonable photocatalytic activity and appropriate dispersion stability due to the higher surface area and the predominance of crystalline anatase phase in silica–titania nanocomposite. In fact, higher surface contact with the dyestuff, where the rhodamine B molecules must be adsorbed by the nanoparticles, leads to more molecules' adsorption on the catalyst surface: thus, higher photo-degradation of dyestuff is resulted. The synthesized $\text{TiO}_2/\text{SiO}_2$ nanocomposites in this study may offer an attractive prospect for applications in self-cleaning coatings.

Acknowledgements The authors would like to acknowledge the financial support provided by Iran Polymer & Petrochemical Institute during the course of this research.

References

- Allen NS, Edge M, Verran J, Stratton J, Maltby J, Bygott C (2008) Photocatalytic titania based surfaces: environmental benefits. *Polym Degrad Stab* 93:1632–1646
- Zhang Y, Pan C (2011) TiO₂/graphene composite from thermal reaction of graphene oxide and its photocatalytic activity in visible light. *J Mater Sci* 46:2622–2626. doi:10.1007/s10853-010-5116-x
- Daoud WA (2013) Self-cleaning materials and surfaces: a nanotechnology approach. Wiley, Chichester
- Nun M, Ball RJ, Bowen ChR, Kurchania R, Sharma GD (2015) Photocatalytic activity of electrophoretically deposited (EPD) TiO₂ coatings. *J Mater Sci* 50:4822–4835. doi:10.1007/s10853-015-9022-0
- Augugliaro V, Loddo V, Pagliaro M, Palmisano G, Palmisano L (2010) Clean by light irradiation practical application of supported TiO₂. RSC Publications, Cambridge
- Ihara T, Miyoshi M, Ando M, Sugihara S, Iriyama Y (2001) Preparation of a visible-light-active TiO₂ photocatalyst by RF plasma treatment. *J Mater Sci* 36:4201–4207. doi:10.1023/A:1017929207882
- Chen X, Mao SS (2007) Titanium dioxide nanomaterials: synthesis, properties, modifications and applications. *Chem Rev* 107:2891–2959
- Fujishima A, Zhang X, Tryk D (2008) TiO₂ photocatalysis and related surface phenomena. *Surf Sci Rep* 63(12):515–582
- Savage N, Diallo MS (2005) Nanomaterials and water purification: opportunities and challenges. *J Nanopart Res* 7:331–342
- Lazar MA, Varghese S, Nair SS (2012) Photocatalytic water treatment by titanium dioxide. *Catalysts* 2:572–601
- Parkin IP, Palgrave RG (2005) Self-cleaning coatings. *J Mater Chem* 15:1689–1695
- Sabzi M, Mirabedini SM, Zohuriaan-Mehr J, Atai M (2009) Surface modification of TiO₂ nano-particles with silane coupling agent and investigation of its effect on the properties of polyurethane composite coating. *Prog Org Coat* 65:222–228
- Pazokifard S, Esfandeh M, Mirabedini SM, Mohseni M, Ranjbar Z (2013) Investigating the role of surface treated titanium dioxide nanoparticles on self cleaning behavior of an acrylic facade coating. *J Coat Technol* 10:175–187
- Allen NS, Edge M, Ortega A, Liauw CM, Stratton J, McIntyre RB (2002) Behaviour of nanoparticle (ultrafine) titanium dioxide pigments and stabilisers on the photooxidative stability of water based acrylic and isocyanate based acrylic coatings. *Polym Degrad Stab* 78:467–478
- Liu Z, Davis RJ (1994) Investigation of the structure of microporous Ti–Si mixed oxides by X-ray, UV reflectance, FT-Raman, and FT-IR spectroscopies. *J Phys Chem* 98:1253–1261
- Murugan K, Rao TN, Rao GVN, Gandhi AS, Murty BS (2011) Effect of dehydration rate on non-hydrolytic TiO₂ thin film processing: structure, optical and photocatalytic performance studies. *Mater Chem Phys* 129:810–815
- Schuisky M, Hårsta A, Aidla A, Kukli K, Kiisler A, Aarik J (2000) Atomic layer chemical vapor deposition of TiO₂ low temperature epitaxy of rutile and anatase. *J Electrochem Soc* 147:3319–3325
- Vives S, Meunier C (2008) Influence of the synthesis route on sol-gel SiO₂–TiO₂ (1:1) xerogels and powders. *Ceram Int* 34:37–44
- Mahltig B, Gutmann E, Meyer DC (2011) Solvothermal preparation of nanocrystalline anatase containing TiO₂ and TiO₂/SiO₂ coating agents for application of photocatalytic treatments. *Mater Chem Phys* 127:285–291
- Zheng YY, Ning R (2003) Effects of nanoparticles SiO₂ on the performance of nanocomposites. *Mater Mater Lett* 57:2940–2944
- Dong W, Sun Y, Ma Q, Zhu L, Hua W, Lu X (2012) Excellent photocatalytic degradation activities of ordered mesoporous anatase TiO₂–SiO₂ nanocomposites to various organic contaminants. *J Hazard Mater* 229–230:307–320
- Huang T, Huang W, Zhou C, Situ Y, Huang H (2012) Superhydrophilicity of TiO₂/SiO₂ thin films: synergistic effect of SiO₂ and phase-separation-induced porous structure. *Surf Coat Technol* 213:126–132
- Kim SK, Chang H, Cho K, Kil DS, Cho SW, Jang HD (2011) Enhanced photocatalytic property of nanoporous TiO₂/SiO₂ micro-particles prepared by aerosol assisted co-assembly of nanoparticles. *Mater Lett* 65:3330–3332
- Aguado J, van Grieken R, López-Munoz MJ, Marugán J (2006) A comprehensive study of the synthesis, characterization and activity of TiO₂ and mixed TiO₂/SiO₂ photocatalysts. *Appl Catal A* 312:202–212
- Rasalingam S, Kibombo HS, Wu CM, Budhi S, Peng R, Baltrusaitis J, Koodali RT (2013) Influence of Ti–O–Si hetero-linkages in the photocatalytic degradation of Rhodamine B. *Catal Commun* 31:66–70
- Tobaldi DM, Tucci A, Škapin AS, Esposito L (2010) Effects of SiO₂ addition on TiO₂ crystal structure and photocatalytic activity. *J Eur Ceram Soc* 30:2481–2490
- Pazokifard S, Mirabedini SM, Esfandeh M, Mohseni M, Ranjbar Z (2012) Silane grafting of TiO₂ nanoparticles: dispersibility and photoactivity in aqueous solutions. *Surf Interface Anal* 44:41–47
- Mazaheri L, Mirabedini SM, Esfandeh M, Pazokifard S (2012) Surface modification of silica nanoparticles with titanium tetraisopropoxide and evaluation of their photocatalytic activity. *Iran J Polym Sci Technol* 25:221–230
- Li Z, Hou B, Xu Y, Wu D, Sun Y, Hu W (2005) Comparative study of sol-gelhydrothermal and sol-gel synthesis of titania-silica composite nanoparticles. *J Solid State Chem* 178:1395–1405
- Mahyar A (2010) Characterization and photocatalytic activity of SiO₂–TiO₂ mixed oxide nanoparticles prepared by sol-gel method. *Indian J Chem* 49:1593–1600
- Vasconcelos DCL (2011) Infrared spectroscopy of titania sol-gel coatings on 316L stainless steel. *Mater Sci Appl* 10:1375–1382
- Shao GN, Hilonga A, Jeon SJ, Lee JE, Elineema G, Quang DV (2013) Influence of titania content on the mesostructure of titania-silica composites and their photocatalytic activity. *Powder Technol* 233:123–130
- Mirabedini A, Mirabedini SM, Babalou AA, Pazokifard S (2011) Synthesis, characterization and enhanced photocatalytic activity of TiO₂/SiO₂ nanocomposite in an aqueous solution and acrylic based coatings. *J Prog Coat* 72:453–460
- Zhu A, Cai A, Yu Z, Zhou W (2008) Film characterization of poly (styrene-butylacrylate-acrylic acid)-silica nanocomposite. *J Colloid Interface Sci* 322:51–58
- Liu Y, Ge C, Ren M, Yin H, Wang A, Zhang D (2008) Effects of coating parameters on the morphology of SiO₂-coated TiO₂ and the pigmentary properties. *Appl Surf Sci* 254:2809–2819
- Xu G, Zheng Z, Wu Y, Feng N (2009) Effect of silica on the microstructure and photocatalytic properties of titania. *Ceram Int* 35:1–5
- Kim JM, Chang SM, Kong SM, Kim KS, Kim J, Kim WS (2009) Control of hydroxyl group content in silica particle synthesized by the sol-precipitation process. *Ceram Int* 35:1015–1019
- Yu J, Wang G, Cheng B, Zhou M (2007) Effects of hydrothermal temperature and time on the photocatalytic activity and microstructures of bimodal mesoporous TiO₂ powders. *Appl Catal B* 69:171–180

39. He C, Tian B, Zhang J (2010) Thermally stable SiO₂-doped mesoporous anatase TiO₂ with large surface area and excellent photocatalytic activity. *J Colloid Interface Sci* 344:382–389
40. Jung K, Park S (1999) Anatase-phase titania: preparation by embedding silica and photocatalytic activity for the decomposition of trichloroethylene. *J Photochem Photobiol A* 127:49–54
41. Hashemi-Nasab R, Mirabedini SM (2013) Effect of silica nanoparticles surface treatment on in situ polymerization of styrene-butyl acrylate latex. *Prog Org Coat* 76:1016–1023
42. Hong SS, Lee MS, Park SS, Lee GD (2003) Synthesis of nano-sized TiO₂/SiO₂ particles in the microemulsion and their photocatalytic activity on the decomposition of nitrophenol. *Catal Today* 87:99–105
43. Park HK, Kim DK, Kim CH (1997) Effect of solvent on titania particle formation and morphology in thermal hydrolysis of TiCl₄. *J Am Ceram Soc* 80:743–749
44. Jung KY, Bin Park S (2000) Enhanced photoactivity of silica-embedded titania particles prepared by sol-gel process for the decomposition of trichloroethylene. *Appl Catal B* 25:249–256
45. Farrokhpay S (2009) A review of polymeric dispersant stabilization of titania pigment. *Adv Colloid Interface Sci* 151:24–32
46. Neppolian B, Celik E, Anpo M, Choi H (2008) Ultrasonic-assisted pH swing method for the synthesis of highly efficient TiO₂ nano-size photocatalysts. *Catal Lett* 125:183–191
47. Siddiqueya IA, Ukajia E, Furusawab T, Satoa M, Suzukia N (2007) The effects of organic surface treatment by methacryloxypropyltrimethoxysilane on the photostability of TiO₂. *Mater Chem Phys* 105:162–168
48. Khataee AR, Kasiri MB (2010) Photocatalytic degradation of organic dyes in the presence of nanostructured titanium dioxide: influence of the chemical structure of dyes. *J Mol Catal A: Chem* 328:8–26
49. Behnajady MA, Modirshahla N (2006) Nonlinear regression analysis of kinetics of the photocatalytic decolorization of an azo dye in aqueous TiO₂ slurry. *Photochem Photobiol Sci* 5:1078–1081